RESEARCH ARTICLE

Generation of elemental fluorine through the electrolysis of copper difluoride at room temperature

Kazuhiko Matsumoto,*[a] Keita Shima,[a] Takuya Sugimoto,[a] Takahiro Inoue,[a] and Rika Hagiwara[a]

[a] Prof. K. Matsumoto, Mr. K. Shima, Mr. T. Sugimoto, Mr. T. Inoue, Prof. R. Hagiwara
Graduate School of Energy Science
Kyoto University
Yoshida, Sakyo-ku, Kyoto 606-8501 (Japan)
E-mail: k-matsumoto@energy.kyoto-u.ac.jp

Supporting information for this article is given via a link at the end of the document.

Abstract: The safe generation of F_2 gas at room temperature using simple cell configurations has been the 'holy grail' of fluorine research for centuries. Thus, to address this issue, we report F_2 gas generation through the electrolysis of CuF_2 in a CsF-2.45HF molten salt without the evolution of H_2 gas. The CuF_2 is selected through a series of thermodynamic and kinetic assessments of possible metal fluorides. Anode assessments on graphite and glass-like carbon demonstrate absence of the anode effect during F_2 gas generation due to stabilized operations at room temperature. Although Ni anode dissolves during electrolysis in the conventional medium-temperature cell, herein, it facilitates stable electrolysis over 100 h, achieving the F_2 gas purity over 99 % with potential operation using one-compartment electrolysis. This work presents a safe and propitious mechanism for high-purity fluorine gas generation for small-scale lab and industrial applications.

Introduction

For years, elemental fluorine has been revered for its remarkable reactivity, which makes it uniquely pertinent in expansive applications ranging from the exploration of new chemistries in pioneering studies to practical operations such as the preparation of inorganic compounds, for instance, hexafluorides (e.g., UF_6 and SF_6), carbon fluorides and noble gas fluorides,[1] the direct fluorination of organic substrates,[1a, 2] as well as in the surface treatment of functional materials.[3] Despite its immense potential, the practical production and use of fluorine are mired by safety issues during handling, limiting the methodologies and materials used.

The advancement of fluorine production has been particularly slow. Despite being envisioned decades earlier, fluorine was first isolated by a French Nobelist, Henri Moissan, in 1886 through the electrolysis of an HF electrolyte containing KF as a supporting electrolyte.[4] Therein, H_2 and F_2 gases were generated at the cathode and anode, respectively, in accordance with Equations. (1) and (2):

$$\text{Cathode: } 2H^+ + 2e^- \rightarrow H_2 \quad (1)$$

$$\text{Anode: } 2F^- \rightarrow F_2 + 2e^- \quad (2)$$

$$\text{Total: } 2HF \rightarrow H_2 + F_2 \quad (3)$$

Notwithstanding the momentous breakthrough by Moissan, it was not until 1986, a hundred years later, that the first chemical synthesis of F_2 gas was achieved through the thermal decomposition of MnF_4 prepared from the Lewis acid-base reaction of K_2MnF_6 and SbF_5, as reported by Christe.[5] In another noteworthy milestone reported by Kraus et al. in 2012, F_2 gas was found to emanate from antozonite, a type of fluorite containing radioactive species, indicating that the elusive halogen gas could be generated through the irradiation of fluorides.[6] More recent works on this topic explored detailed assessments of the crystal structure of F_2 through experimental and theoretical techniques.[7]

Despite the tremendous efforts to industrialize F_2 gas generation, the basic reaction involving the electrolysis of HF, as reported by Moissan, remains unchanged.[8] Advancements in F_2 gas production are mainly focused on electrolyte development to optimize operation temperatures, determine anode material, and improve safety. In the current industrial F_2 production, KF-2HF molten salt at medium temperatures (90 °C) is used under controlled HF dissociation pressure (5×10^3 Pa at 90 °C, the extrapolated value from the data at 98.7, 118.2, and 128.6 °C) and maintained liquid state (melting point 71.7 °C).[9] Carbonaceous materials have found niche utility as anodes on account of their resistivity against oxidation by F_2 gas. Even so, these anode materials are still afflicted by surface fluorination, which results in the so-called "anode effect" characterized by the formation of an insulating film with a small surface energy that causes sharp increases in the anode potential.[8c] For safe deployment, various electrolysis cell configurations have also been developed to ensure complete separation of F_2 and H_2 gases evolved at the anode and cathode, respectively.[8a, 8b]

An alternative approach reported in 1934 proposed the use of CsF-2HF molten salt electrolyte for F_2 gas generation, including metal fluoride electrolysis.[10] In the full phase diagram of the CsF-HF system reported, the liquidus line was found to drop below room temperature around the composition of CsF-2.45HF, indicating the possibility of room-temperature operations.[11] Although a report in 2006 compared the properties of a CsF-2.3HF molten salt with non-volatile ionic liquid [1-alkyl-3-methylimidazolium][$(FH)_{2.3}F$] showing high ionic conductivity and low HF dissociation pressure in the CsF-2.3HF molten salt,[12] successive reports on this Cs system cannot be found. This could be attributed to the high cost of CsF that limits the practicality of the CsF-HF system. However, the growing focus on safety and

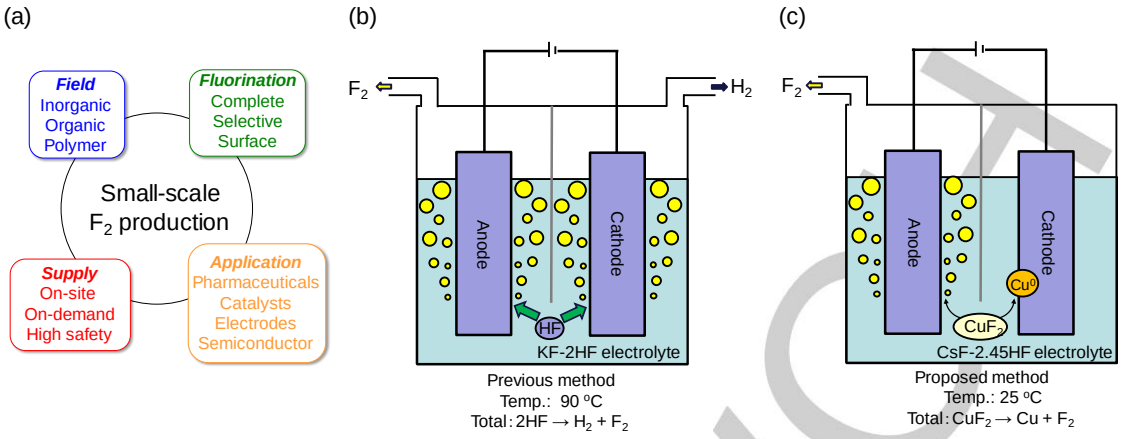

Figure 1. (a) Illustration showing the significance of small-scale F_2 gas production. Schematic drawings of the (b) previous and (c) proposed F_2 gas generation methods. In the previous method, HF is electrolyzed into H_2 and F_2 in the KF-2HF molten salt at 90 °C, whereas the proposed method enables room-temperature electrolysis of CuF_2 with the aid of room-temperature molten salt, CsF-2.45HF. Absence of H_2 gas evolution at the cathode leads to high safety in the proposed method.

the versatility of applications have shifted academic and industrial demands towards *in-situ* and on-demand generation or storage of small quantities of F_2 gas as illustrated by Figure 1(a). At this scale, low currents below 1A could be utilized, minimizing the cost of the CsF-HF system. Most importantly, this approach would provide an avenue for room-temperature generation of F_2 gas without temperature controller.

In a bid to exploit this approach, this study reports the generation of F_2 gas through the electrolysis of CsF-2.45HF molten salt containing CuF_2 at room temperatures. Schematics showing a comparison between the previous F_2 generation processes and the system proposed in this study are furnished in Figure 1 (b) and (c), respectively. We ascertain that the composition of CsF-2.45HF corresponds to the eutectic point in the phase diagram with a eutectic temperature of 16.9 °C.[11] By using CuF_2, H_2 gas evolution at cathode is inhibited, significantly improving the safety of operations while unveiling the possibility of one-compartment electrolysis (electrolysis without partitioning the electrodes by a skirt). Screening of metal fluorides based on thermodynamic calculations, electrode behavior in the cathodic and anodic reactions, confirmation of purity, and possibility of one-compartment electrolysis will be discussed in details.

Results and Discussion

Ionic conductivity and viscosity measurements conducted on CsF-2.45HF revealed a sufficiently high ionic conductivity (86 mS cm^{-1}) and low viscosity (19 mPa s) for electrolysis at 25 °C (cf. ionic conductivity at 25 °C: 109 mS cm^{-1} for 1 mol kg^{-1} aqueous solution of KCl,[13] 14 mS cm^{-1} for a typical ionic liquid, [1-ethyl-3-methylimidazolium][BF_4],[14] and 10.8 mS cm^{-1} for 1 mol dm^{-3} ethylene carbonate/dimethyl carbonate (1:1 in vol.) solution of Li[PF_6][15]). The molten salt was also confirmed to have a low HF dissociation pressure below 1 kPa.

The redox potentials (Figure 2(a)) of selected MF_n/M or MF_n/MF_m (M = Ag, Cu, and Fe) couples were calculated from thermodynamic data (see Table S1, Supporting Information, for estimation of the redox potentials). Although the availability of the redox couples can be obtained by evaluating the overpotential of H_2 gas evolution, in this study, initial estimations were derived from available data for safety. From the thermodynamic data, the AgF/Ag and CuF_2/Cu redox potentials are noted to be above the HF/H_2 redox potential (0.85 and 0.25 V vs. HF/H_2, respectively), whereas the FeF_3/FeF_2, FeF_3/Fe, and FeF_2/Fe exhibit redox potentials below the HF/H_2 redox potential (−0.40, −0.56, and −0.64 V vs. HF/H_2, respectively).

Typically, metal fluorides with higher redox potentials than HF/H_2 are preferred as they are less susceptible to H_2 gas evolution. X-ray fluorescence spectroscopy data indicated the solubilities of AgF, CuF_2, FeF_3, and FeF_2 in CsF-2.45HF to be 2.8×10^{-3}, 2.6×10^{-1}, 1.3×10^{-1}, and 5.6×10^{-2} mol kg^{-1}, respectively. Thus, it can be deduced that AgF and FeF_2, as the metal fluoride candidates for electrolysis in the present process, would be unfavorable due to their low solubilities. Another drawback of using FeF_2 (or other metal fluorides at a low oxidation state) is the possible occurrence of a shuttle effect between the cathode and anode, whereby the metal fluoride at the anode is oxidized, causing deterioration of the anode current efficiency.

To assess the reduction of CuF_2 or FeF_3 in CsF-2.45HF, cyclic voltammograms of a Ni plate electrode were obtained from the respective metal fluoride systems, as shown in Figure 2 (b) and (c). Details of the cell setup and gas line are furnished in the Supporting Information (Figures S1 and S2) and the CsF-2.45HF saturated with metal fluorides was used for this measurements. The electrode potential is referenced to the apparent H_2 gas evolution potential estimated by linearly extrapolating the H_2 gas evolution curve. In the CuF_2-system (Figure 2 (b)), the cathodic wave representing CuF_2 reduction is notably separated from the H_2 gas evolution wave, whereas the FeF_3 reduction and H_2 gas evolution reactions overlap each other in the FeF_3-system (Figure 2 (c)). These observations demonstrate CuF_2 reduction as a

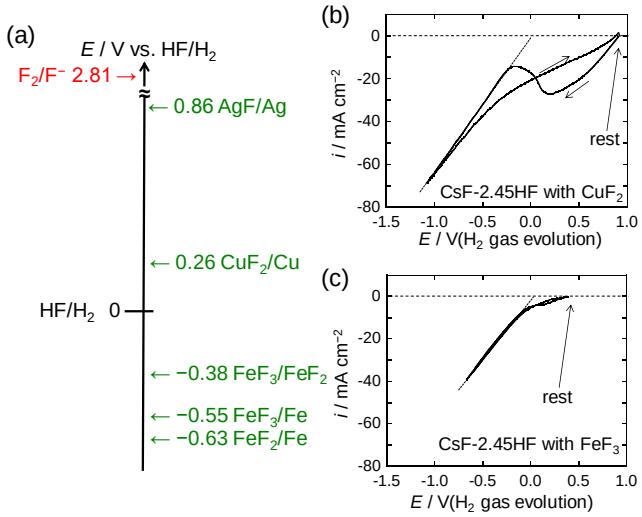

Figure 2. (a) Redox potentials of selected M_xF/M (M: metal) and F_2/F^- couples and cyclic voltammograms of a Ni plate electrode in the CsF-2.45HF molten salt containing (b) CuF_2 and (c) FeF_3 (see Figure S1, Supporting Information, for the cell setup). Metal fluorides were saturated in both the cases. Metal fluorides with redox potentials above HF/H_2 are preferable to avoid H_2 gas generation at the cathode. See Table S1 and related discussion in Supporting Information for thermodynamic estimation of these redox potentials. The potential in the horizontal axis of (b) and (c) is roughly referenced to the potential of H_2 gas evolution by linearly extrapolating the H_2 gas evolution curve. The reduction current of CuF_2 is significantly larger than that of FeF_3 in the range above the H_2 gas evolution potential.

feasible cathodic reaction, while FeF_3 reduction is encumbered by the competitive H_2 gas evolution. Therefore, CuF_2 was selected as the metal fluoride to be electrolyzed in the present process under the following reaction equations (see cyclic voltammograms showing the F_2 gas evolution behavior of glass-like carbon and Ni electrodes in CsF-2.45HF containing CuF_2 in Figure S3):

Cathode: $Cu^{2+} + 2e^- \rightarrow Cu$ (4)

Anode: $2F^- \rightarrow F_2 + 2e^-$ (5)

Total: $CuF_2 \rightarrow Cu + F_2$ (6)

To ascertain the electrodeposition behavior of Cu metal in the present system, potentiostatic electrolysis was performed on a Ni working electrode at −0.5 V vs. CuF_2/Cu (17.3 C cumulatively). A red-brown deposit observed on the electrode was confirmed to be Cu metal through X-ray diffraction (Figure S4). To understand the basic electrochemical behavior of the entire cell, short-term electrolysis (up to 1000s) was performed on the CsF-2.45HF molten salt containing CuF_2 in a 10 cm^3 cell at 100 mA. The potential of the Cu cathode (surface area: 24 cm^2) was maintained between −0.1 and −0.2 V, while that of the glass-like carbon anode (surface area: 4.7 cm^2) was kept around 8 V as long as a sufficient amount of CuF_2 was available (see Figure S5 (a) and (b)). The gas generated at the anode was qualitatively identified as F_2 gas through a reaction with KI (see Figure S6 for the visual change of the KI column). Consumption of over 96 % of CuF_2 was confirmed by monitoring the cathode potential; the cathode potential started to decline to −0.4 V vs. Cu(II)/Cu owing to the deficiency of CuF_2, as the quantity of electricity had reached a theoretical value corresponding to the full consumption of CuF_2 initially added (see Figure S5(c) for the cathode potential profile at the end of electrolysis). The Cu deposit was also noted to grow towards the bottom of the cell because of the electric flux detour around the skirt (see Figure S5 (d)).

A serious problem facing typical F_2 gas generation through the electrolysis of KF-2HF systems utilizing carbon anodes is the so-called “anode effect”, whereby a passivation layer of fluorinated carbon is formed on the surface of the carbon anode,[1d, 16] diminishing the wettability of the electrolyte on the anode. This prevents further F_2 gas generation and results in a sharp rise in the anode potential accompanied by a decrease in the current.[8c] To investigate this phenomenon in the CsF-2.45HF system containing CuF_2 (33.5 g was added to 1 kg of CsF-2.45HF), the average anode potentials of the glass-like carbon, graphite, and Ni electrodes were obtained through galvanostatic electrolysis at current densities in the 100−500 mA cm^{-2} range (5 min for each current density) as shown in Figure 3. In the glass-like carbon electrode cells, a linear increase in the anode potential is observed with increasing current density. No sharp spikes are seen, attributing the behaviour to the influence of DC-IR exclusively. On the other hand, the increasing graphite anode potential with increasing current density becomes even more exacerbated at elevated current densities. However, the occurrence of the “anode effect” was not observed, suggesting that the fluorination of the graphite electrode at high current densities is not drastic enough to cause significantly high resistance at the electrode surface. This observation is contrary to the behavior of graphite electrodes in the KF-2HF molten salt at 90 °C.[8c] After electrolysis, the graphite electrode surface was found to have cracks and exfoliations unlike the glass-like carbon, suggesting the latter facilitates a more stable electrolysis.

For the present electrolysis, the Ni electrode appears to be a more feasible electrode candidate, as it is more economical than the glass-like carbon. Previous works have reported poor F_2 gas generation when a Ni electrode is used in the medium-temperature KF-2HF molten salt electrolysis,[8a, 17] on account of nickel fluoride dissolution into the electrolyte that causes sludge deposition in the cell. However, in the present system, the low

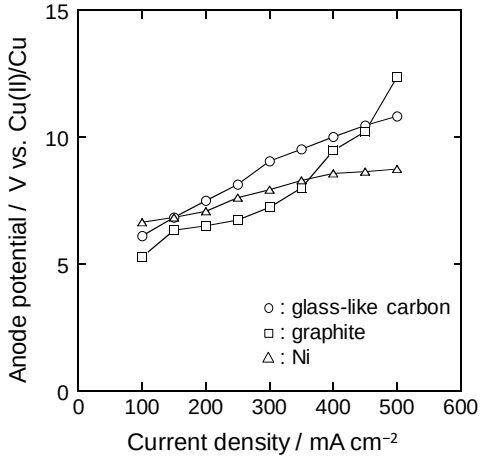

Figure 3. Average anode potentials of the glass-like carbon, graphite, and Ni electrodes during galvanostatic electrolysis of the CsF-2.45HF molten salt electrolyte containing CuF_2 (CuF_2 saturated) (5 min for each current density from 100 to 500 mA). The anode effect, characterized by a sharp increase in the anode potential, is not observed in all cases.

solubility of nickel fluorides at room temperature and the high kinetic barrier of nickel fluoride formation played critical roles in its utilization as an anode material. A similar mechanism occurs in the Simons process, where a Ni electrode effectively works as an anode in anhydrous HF at room temperature to oxidize organic compounds.[18]

For further insight into the electrolytic behavior of the present system, in-depth investigations (quantitative analysis, purity test, and long-term electrolysis) were performed on a larger cell (100 cm^3) comprising a Cu mesh cathode (apparent surface area 60 cm^2), a Cu wire reference electrode, and a Ni anode (7.0 cm^2) immersed in CsF-2.45HF containing CuF_2 as shown in the schematic diagram (Figure S7).

Quantitative analysis was performed by measuring the volume of the gas evolved at the anode. Although the two-electron per gas molecule process (Equation 5) can be used to calculate the volume of F_2 gas evolved at the anode, possible side reactions causing gas evolution (O_2 or OF_2 gas) could occur at the anode due to H_2O contamination. The side reactions entailing four electrons per gas molecule in accordance with Equations (7) and (8) would lead to lower volumes of F_2 gas than envisioned in Equation 5. Therefore, to estimate the efficiency of F_2 gas evolution in the present system, gas volume measurements would be necessary.

$$2H_2O \rightarrow O_2 + 4H^+ + 4e^- \quad (7)$$

$$H_2O + 2HF \rightarrow OF_2 + 4H^+ + 4e^- \quad (8)$$

The volume of the gas evolved at the Ni anode during galvanostatic electrolysis of CuF_2 in CsF-2.45HF at 200 mA was measured using a PFA gas burette with poly(chlorotrifluoroethylene) oil. The relationship between the gas volume and the electrolysis duration (time) is shown in Figure 4(a). The gas volume is proportional to electrolysis duration with a slight deviation from the ideal line, in accordance with Faraday's law, which suggests a lower efficiency possibly resulting from the above-mentioned side reactions. Infrared spectrum of the F_2 gas evolved at the anode identified a very limited amount of OF_2 impurity (see Figure S8 for the IR spectrum with that before pre-electrolysis. Note that O_2 gas cannot be detected through infrared spectroscopy). The Central Glass method,[19] using UV-visible spectroscopy based on the absorption of F_2 gas at ~280 nm, was employed for a more accurate evaluation of F_2 gas purity.[20] Figure 4 (b) shows the UV-visible spectrum of the F_2 gas obtained from electrolysis at 200 mA alongside a typical spectrum of cylinder-supplied F_2 gas. A comparison of the integrated areas of the absorption peaks revealed the purity of generated F_2 gas to be 99 %.

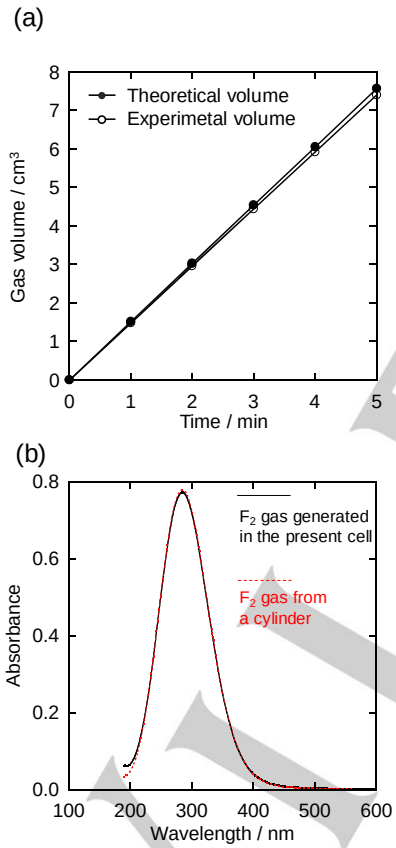

Figure 4. Relationship between the electrolysis duration (time) and the volume of the gas generated at the anode during galvanostatic electrolysis of the CsF-2.45HF molten salt electrolyte containing CuF_2 (CuF_2 saturated) at 200 mA cm^{-2}. Surface area: 7.0 cm^2 for the Ni plate anode and 60 cm^2 for the Cu mesh cathode. The gas volume was measured by an F_2-resistant gas burette. (b) An ultraviolet-visible spectrum of F_2 gas (black) generated through the present method using the Ni electrode in the CsF-2.45HF molten salt electrolyte containing CuF_2. Surface area: 7.0 and 60 cm^2 for the Ni anode and Cu cathode, respectively. The purity was calculated based on the calibration using F_2 gas (red) from a commercial cylinder (purity 99 %). Gas pressure: 40 kPa. The F_2 gas was generated by galvanostatic electrolysis at 200 mA for 45 min using the 100 cm^3 cell (Figure S7). See the literature for the details on the Central Glass method and UV-vis spectrum of F_2 gas.[1-4]

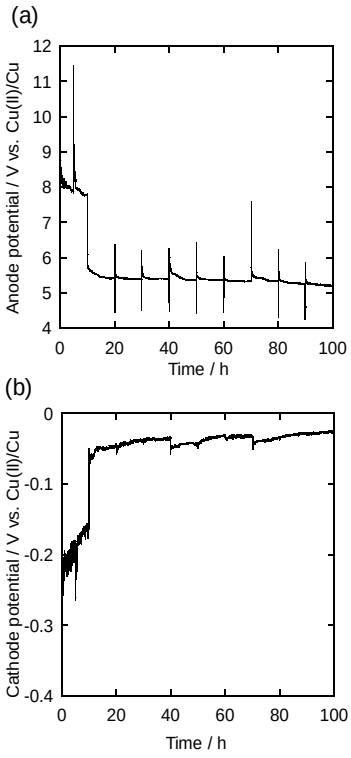

Figure 5. (a) Anode and (b) cathode potentials during long-term intermittent galvanostatic electrolysis of the CsF-2.45HF molten salt electrolyte containing CuF_2 (CuF_2 saturated) for 100 h (5 h × 2 at 500 mA and 10 h × 9 at 100 mA) in the 100-cm^3 electrolytic cell. Surface area: 7.0 cm^2 for the Ni plate anode and 60 cm^2 for the Cu mesh cathode.

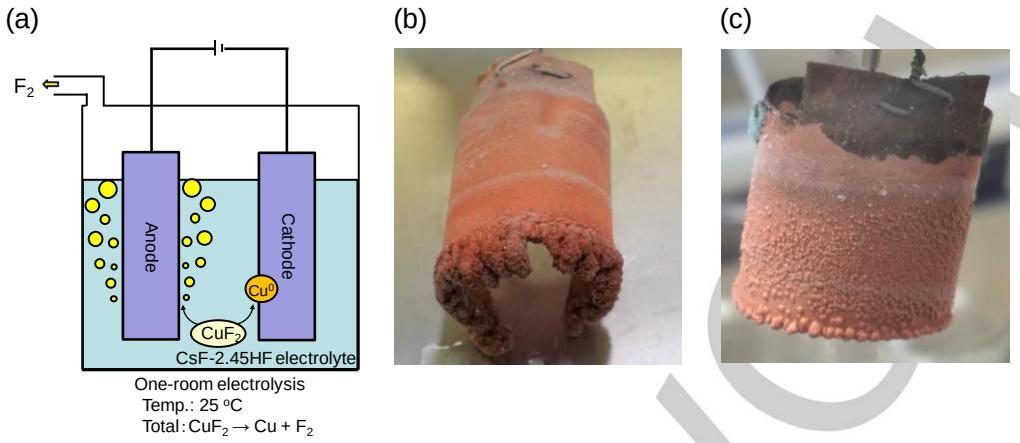

Figure 6. (a) A schematic drawing of a one-compartment electrolytic cell (100 cm^3) comprising CsF-2.45HF molten salt containing CuF_2 (CuF_2 saturated). The cell configuration is similar to the one in Figure 1 (c), with the distinction of the partitioning skirt between the cathode and anode. This setup results in significantly reduced bulk resistance, as shown in Figure S10. An image of Cu metal deposited on the cathode (b) after 100-hour electrolysis with a skirt (Figure 1 (c) and Figure 5 (b)) and (c) after 40-hour electrolysis without a skirt (Figure 6 (a) and Figure S9 (b)).

.

Long term analysis of the large (100 cm^3) cell was conducted for 100 h (current: 500 mA for the first 10 h and 100 mA for 90 h thereafter). The electrolysis was performed for 5 h per day for the initial 10 h followed by 10 h per day for the subsequent 90 h, for 9 days to demonstrate the possible intermittent operation in practical cells. The resulting Ni anode and Cu cathode potentials are shown in Figure 5 (a) and (b). Although the anode potential is observed to spike at the beginning of each electrolysis (due to high resistance at the electrode surface), it promptly decreases in a short period. Electrolysis at 500 mA is characterized by a gradual decrease in the anode potential, which stabilizes between 5.5 and 5.0 V at 100 mA with no sign of the anode effect. The cathode potential remains above −0.3 V at 500 mA and over −0.1 V at 100 mA, suggesting safe electrolysis with no generation of H_2 gas (see Figure 2(b)).

Since H_2 gas is not generated at the cathode and the reaction between the Cu metal and F_2 gas is negligible, one-compartment electrolysis (wherein the skirt between the cathode and anode is removed) can be accomplished in the present system (see Figure 6(a) and Figure S7(a) in the Supporting Information, for the schematic drawing of the one-compartment electrolysis cell). Although this electrolysis cell requires strict monitoring of the cathode potential to ensure no H_2 gas is evolved for safety reasons, the simplified cell construction and the reduced ohmic drop caused by electrolyte bulk resistance makes it advantageous to implement. Moreover, without the skirt which geometrically drives current concentration to the bottom part of the electrodes, a larger effective electrode area can be achieved, reducing the actual current density at both electrodes.

A trial of the one-compartment electrolysis using the 100-cm^3 cell over 40 h at 100 mA demonstrated stable electrode potentials (see Figure S9 for detailed electrochemical behavior). Electrochemical impedance spectroscopy performed on cells with and without the skirt revealed a significant difference in the ohmic drops of the Ni electrodes (7.5 Ω with a skirt and 1.7 Ω without a skirt), affirming the electrochemical benefit of the one-compartment electrolysis (Figure S10 for the Nyquist plots of the electrochemical systems with and without the skirt). A closer inspection of the Cu metal deposition on the Ni electrodes from the cells with and without the skirt reveals bulkier deposition at the bottom of the electrode used with the skirt (Figure 6 (b)), indicative that the current flows from the bottom to avoid the skirt. On the other hand, the electrode used without the skirt, portrays a uniform distribution of Cu metal deposit on the entire cathode, indicating a more homogeneous current flow between cathode and anode (Figure 6 (c)).

Conclusion

In this study, we report room temperature F_2 gas generation for small-scale lab and industry applications. With simple peripheral equipment, $Cs[(FH)_{2.45}F]$ molten salt, which was reported over 80 years ago, facilitates F_2 gas generation upon addition of CuF_2. Preliminary screening of selected metal fluorides demonstrates improved safety when CuF_2 is utilized as it prevents H_2 gas generation. Although the anode effect does not occur on graphite and glass-like carbon electrodes even at high current densities during electrolysis, a slight increase in the anode potential is observed in graphite, suggesting the occurrence of surface fluorination. Herein we note that unlike in medium-temperature KF-2HF molten salt cells, the Ni electrode exhibits a stable electrolysis behavior in $Cs[(FH)_{2.45}F]$ owing to its low solubility at room temperature. Besides, higher durability and lower cost make it a more auspicious electrode choice. The proposed electrolysis cell not only demonstrates stable intermittent electrolysis of CuF_2 performed over 100 h but also generated F_2 gas with a high purity of 99%, albeit with traces of OF_2 impurity. For prolonged F_2 gas generation, strategies such as replenishing CuF_2 upon depletion (provided it is handled under dry conditions) or replacing the entire electrolytic cell (mechanical exchange), could be undertaken. Recovery of the cathodically

deposited Cu metal to CuF_2 may be an important process from a certain scale of generation. Although the theoretical amount and maximum rate of F_2 gas generated in the present 100-cm^3 cell is 2.28 dm^3 and 0.232 dm^3 h^{-1}, respectively (see Supporting Information for their estimation), it can be increased by scaling up the cell and electrode sizes, depending on the type of application. Compared with the previously known chemical synthesis of F_2 (see Introduction for details), which is also a possible method for small-scale production, facile control of the amount of F_2 gas by electrochemical parameters is a significant advantage of the present method. The gas generation process without directly handling reactive fluorides such as SbF_5 is also beneficial in some practical use.

We believe that this facile electrolysis process is a groundbreaking approach to small-scale and on-demand F_2 gas generation that will open up new horizons for the exploration and utilization of F_2 gas in a wide range of domains such as fundamental studies in fluorine chemistry, direct fluorination of organic compounds, and surface treatment of functional materials including semi-conductors. Future works focused on improving the proposed cell configuration and expanding the fields of F_2 gas are highly expected.

Acknowledgements

This work was supported by JSPS KAKENHI Grant Number 17K19175. The authors thank Ueki Corporation for the cell design and Central Glass Co., Ltd. for the F_2 purity test.

Keywords: Fluorine • Fluorides • Electrolysis • Small-scale production

[1] (a) H. W. Roesky, *Efficient Preparations of Fluorine Compounds*, John Wiley & Sons, Hoboken, **2013**; (b) K. Seppelt, *Chem. Rev.* **2015**, *115*, 1296-1306; (c) P. Laszlo, G. J. Schrobilgen, *Angew. Chem. Int. Ed.* **1988**, *27*, 479-489; *Angew. Chem.* **1988**, *100*, 495-506; (d) O. V. Boltalina, T. Nakajima, *New Fluorinated Carbons: Fundamentals and Applications*, 1st, ed. A. Tressaud (Series Ed.), Elsevier, London, **2016**.

[2] (a) G. Sandford, *J. Fluorine Chem.* **2007**, *128*, 90-104; (b) C. B. McPake, G. Sandford, *Org. Process. Res. Dev.* **2012**, *16*, 844-851; (c) D. D. DesMarteau, *J. Fluorine Chem.* **2006**, *127*, 1467-1470; (d) P. A. Champagne, J. Desroches, J. D. Hamel, M. Vandamme, J. F. Paquin, *Chem. Rev.* **2015**, *115*, 9073-9174; (e) R. D. Chambers, J. Hutchinson, G. Sandford, *J. Fluorine Chem.* **1999**, *100*, 63-73.

[3] (a) A. Tressaud, E. Durand, C. Labrugere, A. P. Kharitonov, L. N. Kharitonova, *J. Fluorine Chem.* **2007**, *128*, 378-391; (b) V. Dybbert, S. M. Fehr, F. Klein, A. Schaadt, A. Hoffmann, E. Frei, E. Erdem, T. Ludwig, H. Hillebrecht, I. Krossing, *Angew. Chem. Int. Ed.* **2019**, *58*, 12935-12939; *Angew. Chem.* **2019**, *131*, 13069-13073.

[4] (a) H. R. Moissan, *C. R. Hebd. Seances Acad. Sci.* **1886**, *75*, 1543–1544; (b) H. R. Moissan, *C. R. Hebd. Seances Acad. Sci.* **1886**, *103*, 202-205; (c) M. E. Weeks, *J. Chem. Educ.* **1932**, *9*, 1915-1939; (d) A. Tressaud, *Angew. Chem. Int. Ed.* **2006**, *45*, 6792-6796; *Angew. Chem.* **2006**, *118*, 6946-6950.

[5] K. O. Christe, *Inorg. Chem.* **1986**, *25*, 3721-3722.

[6] (a) J. S. A. D. Gunne, M. Mangstl, F. Kraus, *Angew. Chem. Int. Ed.* **2012**, *51*, 7847-7849; *Angew. Chem.* **2012**, *124*, 7968-7971; (b) V. R. Celinski, M. Ditter, F. Kraus, F. Fujara, J. S. A. D. Guenne, *Chem. Eur. J.* **2016**, *22*, 18388-18393.

[7] (a) S. Mattsson, B. Paulus, F. A. Redeker, H. Beckers, S. Riedel, C. Muller, *Chem. Eur. J.* **2019**, *25*, 3318-3324; (b) S. I. Iviev, A. J. Karttunen, M. Hoelzel, M. Conrad, F. Kraus, *Chem. Eur. J.* **2019**, *25*, 3310-3317.

[8] (a) R. J. Ring, D. Royston, *A Review of Fluorine Cells and Fluorine Production Facilities, in Australian Atomic Energy Commission Research Estrablishment, Lucus Heights*, **1973**; (b) G. H. Cady, D. A. Rogers, C. A. Carlson, *Ind. Eng. Chem.* **1942**, *34*, 443-448; (c) H. Groult, *J. Fluorine Chem.* **2003**, *119*, 173-189.

[9] G. H. Cady, *J. Am. Chem. Soc.* **1934**, *56*, 1431-1434.

[10] F. C. Mathers, P. T. Stroup, *Trans. Am. Electrochem. Soc* **1934**, *66*, 245-252.

[11] R. V. Winsor, G. H. Cady, *J. Am. Chem. Soc.* **1948**, *70*, 1500-1502.

[12] (a) K. Matsumoto, J. Ohtsuki, R. Hagiwara, S. Matsubara, *J. Fluorine Chem.* **2006**, *127*, 1339-1343; (b) S. Kohara, M. Takata, K. Matsumoto, R. Hagiwara, K. Suzuya, H. Morita, J. E. Siewenie, C. J. Benmore, *J. Chem. Phys.* **2008**, *129*; (c) R. Hagiwara, Y. Nakamori, K. Matsumoto, Y. Ito, *J. Phys. Chem. B* **2005**, *109*, 5445-5449; (d) R. Hagiwara, K. Matsumoto, Y. Nakamori, T. Tsuda, Y. Ito, H. Matsumoto, K. Momota, *J. Electrochem. Soc.* **2003**, *150*, D195-D199.

[13] K. W. Pratt, W. F. Koch, Y. C. Wu, P. A. Berezansky, *Pure. Appl. Chem.* **2001**, *73*, 1783-1793.

[14] A. Noda, K. Hayamizu, M. Watanabe, *J. Phys. Chem. B* **2001**, *105*, 4603–4610.

[15] L. Niedzicki, S. Grugeon, S. Laruelle, P. Judeinstein, M. Bukowska, J. Prejzner, P. Szczecinski, W. Wieczorek, M. Armand, *J. Power Sources* **2011**, *196*, 8696-8700.

[16] (a) N. Watanabe, T. Nakajima, H. Touhara, *Graphite Fluorides*, Elsevier, Amsterdam, **1988**; (b) A. Hamwi, K. Guérin, M. Dubois, *Fluorine-intercalated Graphite for Lithium Batteries*, Ch. 17, in *Fluorinate Materials for Energy Conversion* T. Nakajima, H. Groult (Ed.), Elsevier, Oxford, **2005**, pp. 369-395.

[17] H. R. Neumark, *Trans. Electrochem. Soc.* **1947**, *91*, 367-385.

[18] (a) L. Conte, G. P. Gambaretto, *J. Fluorine Chem.* **2004**, *125*, 139-144; (b) M. Drisch, L. A. Bischoff, J. A. P. Sprenger, P. T. Hennig, R. Wirthensohn, J. Landmann, S. Z. Konieczka, M. Hailmann, N. V. Ignat'ev, M. Finze, *Chem. Eur. J.* **2020**, *26*, 11625-11633.

[19] (a) T. Miyazaki, I. Mori, T. Umezaki, S. Yonezawa, *J. Fluorine Chem.* **2019**, *219*, 55-61; (b) I. Mori, M. Kaichi, Japanese Pat. JPB2008-4211983, **2008**.

[20] (a) R. K. Steunenberg, R. C. Vogel, *J. Am. Chem. Soc.* **1956**, *78*, 901-902; (b) R. Holland, J. L. Lyman, *J. Quant. Spectrosc. Radiat. Trans.* **1987**, *38*, 79-80.

Entry for the Table of Contents

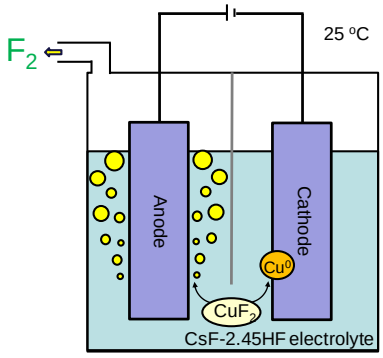

Fluorine gas generation is achieved at room temperature through the electrolysis of CuF_2 in a CsF-2.45HF molten salt without the evolution of H_2 gas. Stable electrolysis with a Ni anode over 100 h (F_2 purity over 99 %) with potential operation using one-compartment electrolysis lead to a safe and propitious mechanism for high-purity fluorine gas generation for small-scale lab and industrial applications.